

# Hierarchical Concept-to-Appearance Guidance for Multi-Subject Image Generation

Yijia Xu <sup>\*1</sup> Zihao Wang <sup>\*2</sup> Jinshi Cui <sup>1</sup>

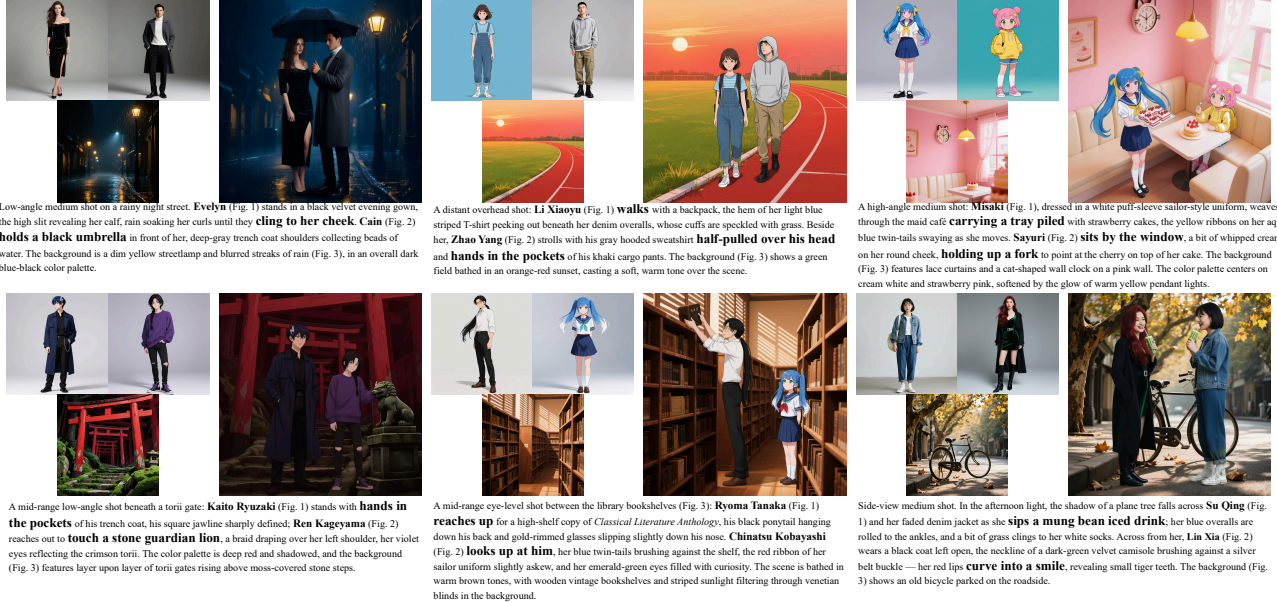


Figure 1. Our multi-character, scene-referenced generation examples show that the outputs not only preserve consistency across characters and scenes, but also faithfully follow the specified action prompts (in bold).

## Abstract

Multi-subject image generation aims to synthesize images that faithfully preserve the identities of multiple reference subjects while following textual instructions. However, existing methods often suffer from identity inconsistency and limited compositional control, as they rely on diffusion models to implicitly associate text prompts with reference images. In this work, we propose Hierarchical Concept-to-Appearance Guidance (CAG), a framework that provides explicit, structured supervision from high-level concepts to fine-grained appearances. At the conceptual level, we introduce a VAE dropout training strategy that randomly omits reference VAE features, encouraging the model to rely more on robust

semantic signals from a Visual Language Model (VLM) and thereby promoting consistent concept-level generation in the absence of complete appearance cues. At the appearance level, we integrate the VLM-derived correspondences into a correspondence-aware masked attention module within the Diffusion Transformer (DiT). This module restricts each text token to attend only to its matched reference regions, ensuring precise attribute binding and reliable multi-subject composition. Extensive experiments demonstrate that our method achieves state-of-the-art performance on the multi-subject image generation, substantially improving prompt following and subject consistency.

## 1. Introduction

Multi-subject generation aims to synthesize images that follow user-provided editing instructions while faithfully preserving the identities of all referenced subjects. In prac-

<sup>1</sup>School of Intelligence Science and Technology, Peking University, Beijing, China <sup>2</sup>The Hong Kong University of Science and Technology, Hong Kong, China. Correspondence to: Jinshi Cui <cjs@cis.pku.edu.cn>.

tical applications such as AI-driven drama production and personalized story illustration, the reference inputs typically comprise multiple characters embedded within complex scenes, while user instructions are often provided as short and concise text. Despite their brevity, such instructions usually imply rich semantic intent, spanning spatial relationships, appearance consistency, and role-specific behaviors. Establishing reliable correspondences between high-level user intent and the fine-grained visual details contained in multiple reference images therefore remains a fundamental challenge.

Recent advances strive to improve subject consistency by refining training objectives. UMO (Cheng et al., 2025) adopts a multi-identity reward learning strategy to enhance identity preservation, whereas MOSAIC (She et al., 2025) enforces cross-image alignment by supervising reference-to-target attention through correspondence masks. However, these approaches mainly regulate the training stage and lack explicit mechanisms that guide the inference process, leading to suboptimal controllability during generation. Moreover, a single DiT (Peebles & Xie, 2023) backbone struggles to handle complex multimodal reasoning when scaling to diverse real-world personalized generation scenarios.

To mitigate the limitations of DiT-only pipelines, several recent works incorporate vision-language models (VLMs). Frameworks such as OmniGen2 (Wu et al., 2025b) and Qwen-Image (Wu et al., 2025a) encode both reference images and user instructions with a VLM before injecting the extracted multimodal features into a DiT backbone. While these methods benefit from the semantic richness of VLM encodings, they typically treat the VLM as a passive feature extractor rather than an active reasoning module. Consequently, they fail to fully leverage the VLM’s capacity for semantic grounding and cross-modal alignment.

A core issue persists across existing pipelines: they rely heavily on the DiT backbone to implicitly associate high-level textual instructions with visual cues from multiple reference images. As the number and diversity of references increase, such implicit alignment becomes unreliable. Even when VLM features are included, there remains no principled mechanism to bridge the semantic representations encoded by the VLM with the fine-grained visual features encoded by the VAE. As a result, DiT must infer cross-modal correspondences without explicit structural guidance, leading to unstable identity binding and degraded compositional consistency. Furthermore, while VLM-derived image features inherently contain rich semantic attributes—such as shape, color, and contextual relations—these informative signals are often overshadowed by the model’s over-reliance on low-level VAE features, limiting semantic expressiveness and compositional controllability. As shown in Figure 2, removing reference-image VAE features during inference of



Figure 2. Qualitative comparison of OmniGen2 (Wu et al., 2025b) under inference with and without using VAE features from reference images.

OmniGen2 (Wu et al., 2025b) leads to inconsistencies not only in fine-grained details but also in semantic attributes such as shape and color. This observation suggests that the model lacks sufficient capability to effectively utilize VLM features. Effectively integrating the complementary strengths of VLM semantics and VAE fine-grained appearance cues therefore remains an open challenge for multi-subject generation.

To address these limitations, we propose Hierarchical Concept-to-Appearance Guidance (CAG), a multi-subject generation framework that explicitly directs the DiT to perform fine-grained text-to-reference correspondence. CAG leverages a VLM to establish dense word-to-region alignments between editing instructions and reference images, providing explicit semantic grounding. During both training and inference, the DiT is equipped with correspondence-aware masked attention at every layer, constraining each textual token to attend only to the VAE features of its matched reference regions while simultaneously attending to target-image features and VLM-encoded text features. This design filters out irrelevant visual and semantic signals, delivering interpretable and consistent alignment supervision throughout the generative process. Moreover, to further exploit the VLM’s semantic reasoning capabilities, we introduce a VAE dropout strategy that randomly omits reference VAE features during training. By forcing the model to rely solely on VLM-encoded features, CAG strengthens its conceptual grounding and enhances its robustness in scenarios where low-level visual cues are sparse or noisy.

Our main contributions are summarized as follows:

- We propose **CAG**, a Hierarchical Concept-to-

Appearance Guidance framework for multi-subject image generation, which explicitly incorporates VLM knowledge into diffusion models through concept-level and appearance-level conditioning.

- At the *conceptual level*, we introduce a VAE dropout training strategy that randomly omits reference VAE features, encouraging the model to rely more strongly on VLM-derived semantic representations and improving its robustness to incomplete low-level visual cues.
- At the *appearance level*, we employ correspondence-aware masked attention within the DiT backbone, constraining each text token to attend only to its matched reference regions and associated VLM features, thereby enabling precise, localized attribute binding and reliable multi-subject composition.
- Extensive experiments demonstrate that **CAG** consistently outperforms existing methods on multi-subject generation tasks involving diverse human identities and scene references, achieving state-of-the-art performance in text fidelity, identity preservation, and compositional quality.

## 2. Related Work

### 2.1. Multi-subject Driven Image Generation

Recent advances in image editing models (Zhang et al., 2023b; Sheynin et al., 2023; Deng et al., 2025; Batifol et al., 2025; Brooks et al., 2023; Xia et al., 2024; Ge et al., 2024; Wu et al., 2025a; Tan et al., 2025; Chen et al., 2025a; Gal et al., 2022; Ruiz et al., 2023) have shown remarkable progress. Building upon single-subject generation approaches, a series of multi-subject generation methods have been developed to support reference-guided customization. UNO (Wu et al., 2025c) introduces a model–data co-evolution strategy to enable consistent generation across multiple references. DreamOmni2 (Xia et al., 2025) carefully constructs a three-stage data creation pipeline to acquire high-quality multi-reference training data. DreamO (Mou et al., 2025) computes the loss based on the attention between condition images and the generated image, while MOSAIC (She et al., 2025) introduces two additional losses that respectively utilize reference-to-target latent attention and inter-reference attention to further improve cross-image consistency. UMO (Cheng et al., 2025) advances this line of research by proposing a multi-identity matching reward that reinforces subject-level consistency.

### 2.2. Multimodal Understanding for Reference-Guided Generation

Multi-subject generation involves both visual and textual inputs, requiring strong multimodal understanding capabili-

ties from the model. Recent studies have developed unified models (Team, 2025; Deng et al., 2025; Li et al., 2025; Chen et al., 2025b; Cao et al., 2025; Chen et al., 2025c) that integrate both visual understanding and image generation within a single framework. Some approaches focus on extracting cross-image relationships (Lee et al., 2019; 2020; Lu et al., 2024; Lowe, 2004; Bay et al., 2006; Tang et al., 2023; Zhang et al., 2023a; 2024). Another line of work (Wu et al., 2025b;a) leverages pretrained vision–language models (VLMs) (Bai et al., 2025; Wang et al., 2024) for their superior multimodal representation ability, feeding both VLM-encoded reference image and text features, along with VAE-encoded visual features, into subsequent diffusion transformers (DiTs).

## 3. Methodology

### 3.1. Preliminary

Given a set of  $N$  reference images  $\{I_i^r\}_{i=1}^N$  and a textual editing instruction  $t^e$ , the goal of the multi-subject image generation task is to synthesize a target image  $I^t$  that follows the instruction while preserving and compositing the visual contents from the reference images. Formally, the task can be expressed as

$$I^t = \mathcal{F}(\{I_i^r\}_{i=1}^N, t^e), \quad (1)$$

where  $\mathcal{F}(\cdot)$  denotes the conditional image generation process.

In a typical VLM–DiT framework, a Vision–Language Model (VLM) is employed to extract multi-modal representations by jointly encoding each reference image and the textual instruction:

$$\mathbf{h}_i^r, \mathbf{h}^e = \text{VLM}([I_i^r, t^e]), \quad i = 1, \dots, N. \quad (2)$$

Here,  $\mathbf{h}_i^r$  represents the visual features associated with the  $i$ -th reference image, and  $\mathbf{h}^e$  denotes the text-conditioned semantic representation that provides instruction-aware guidance.

Meanwhile, each reference image is also encoded by a VAE encoder to obtain its low-level latent representation:

$$\mathbf{v}_i^r = \text{VAE}_{\text{enc}}(I_i^r), \quad i = 1, \dots, N. \quad (3)$$

The representations  $\{\mathbf{h}_i^r\}$ ,  $\mathbf{h}^e$ , and  $\{\mathbf{v}_i^r\}$  serve as conditioning signals for the DiT-based denoising network, which synthesizes the target image  $I^t$  by integrating semantic guidance from the VLM and fine-grained visual details from the VAE latents.

In the DiT-based architecture, multi-modal features from both the reference and target domains are jointly attended to within each transformer layer. Specifically, at every layer  $\ell$

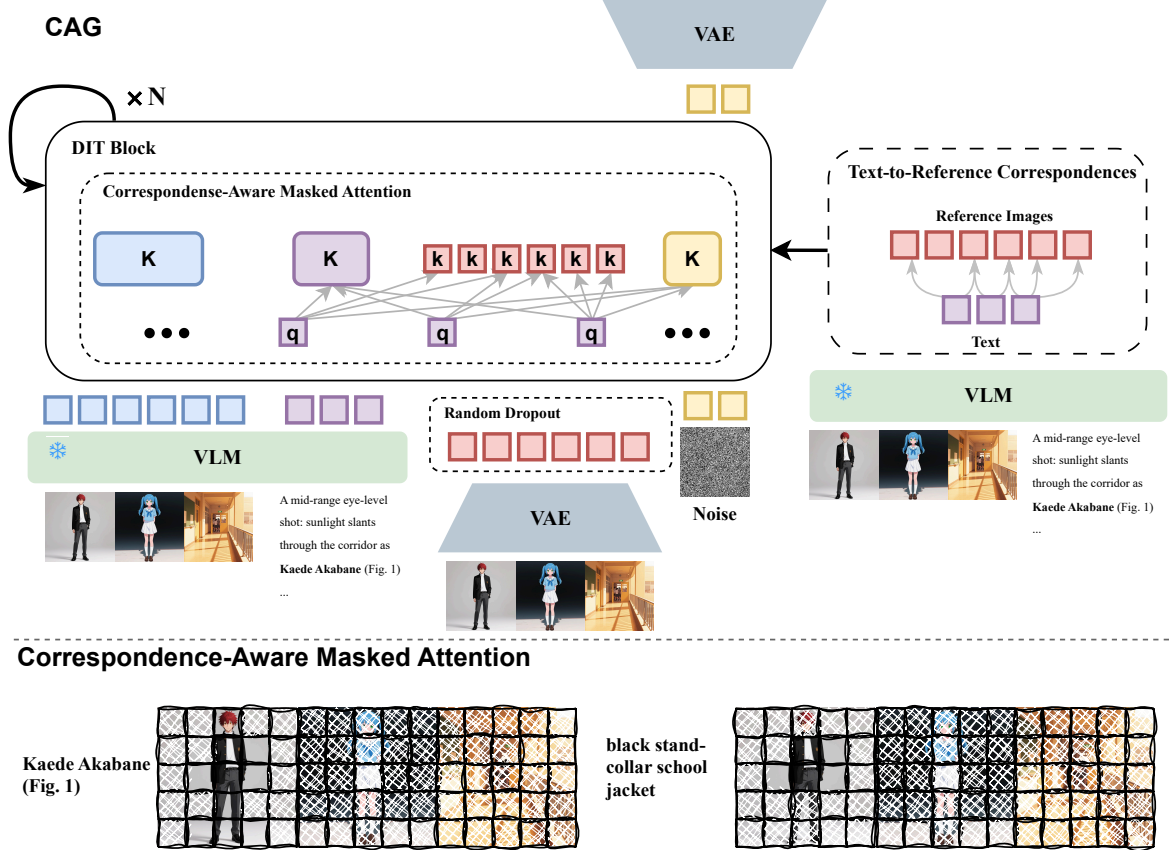


**Figure 3. Overview of CAG.** **Top:** The overall training pipeline of our CAG framework, which integrates the proposed VAE Dropout strategy and the Correspondence-Aware Masked Attention mechanism. **Bottom:** Illustration of the proposed Correspondence-Aware Masked Attention, where text tokens are explicitly matched to their associated regions in the reference images, enabling fine-grained and identity-consistent multi-subject generation.

of the DiT, the query, key, and value representations from the reference-image VLM features, the text VLM features, the target-image VAE features, and the reference-image VAE features are concatenated and processed through a unified self-attention operation.

Formally, let  $\mathbf{Q}^{(\ell)}$ ,  $\mathbf{K}^{(\ell)}$ , and  $\mathbf{V}^{(\ell)}$  denote the query, key, and value matrices in the  $\ell$ -th attention layer. They are constructed as

$$\begin{aligned} \mathbf{Q}^{(\ell)} &= [\mathbf{Q}_{\text{VLM}}^r, \mathbf{Q}_{\text{VLM}}^e, \mathbf{Q}_{\text{VAE}}^t, \mathbf{Q}_{\text{VAE}}^r], \\ \mathbf{K}^{(\ell)} &= [\mathbf{K}_{\text{VLM}}^r, \mathbf{K}_{\text{VLM}}^e, \mathbf{K}_{\text{VAE}}^t, \mathbf{K}_{\text{VAE}}^r], \\ \mathbf{V}^{(\ell)} &= [\mathbf{V}_{\text{VLM}}^r, \mathbf{V}_{\text{VLM}}^e, \mathbf{V}_{\text{VAE}}^t, \mathbf{V}_{\text{VAE}}^r], \end{aligned} \quad (4)$$

where  $[\cdot]$  denotes concatenation along the token dimension.

The self-attention for layer  $\ell$  is then computed as

$$\mathbf{A}^{(\ell)} = \text{Softmax} \left( \frac{\mathbf{Q}^{(\ell)} (\mathbf{K}^{(\ell)})^\top}{\sqrt{d}} \right) \mathbf{V}^{(\ell)}, \quad (5)$$

where  $d$  is the feature dimension. This unified attention mechanism enables the DiT to perform cross-modal reasoning among four types of representations — reference-image

VLM features ( $\mathbf{VLM}^r$ ), instruction VLM features ( $\mathbf{VLM}^e$ ), reference-image VAE features ( $\mathbf{VAE}^r$ ), and target-image VAE features ( $\mathbf{VAE}^t$ ) — allowing the network to jointly integrate semantic and visual information at every layer.

### 3.2. VAE Dropout Training Strategy

The image features encoded by the VLM,  $\mathbf{h}_i^r$ , contain rich semantic information, analogous to detailed textual descriptions. However, during text-conditional pretraining, the DiT has only learned to follow textual guidance and is not trained to directly leverage the VLM-encoded image features. DiT, being familiar with the VAE features from pretraining, tends to over-rely on  $\mathbf{v}_i^r$  at the beginning of training, preventing it from effectively exploiting  $\mathbf{h}_i^r$ .

To mitigate this issue, we propose a VAE dropout training strategy. During training, with a certain probability, the DiT is prevented from using the VAE-encoded reference features  $\mathbf{v}_i^r$  and relies solely on the VLM-encoded textual and image features  $\mathbf{h}_i^r$  to compute the loss. Formally, let  $p$  denote the dropout probability; for a given training step, the

input features to DiT are:

$$\{\mathbf{v}_i^r, \mathbf{h}_i^r, \mathbf{h}^e\} \rightarrow \begin{cases} \{\mathbf{v}_i^r, \mathbf{h}_i^r, \mathbf{h}^e\}, & \text{with } 1-p, \\ \{\mathbf{h}_i^r, \mathbf{h}^e\}, & \text{with } p. \end{cases} \quad (6)$$

This forces the DiT to learn to extract detailed semantic information from the VLM-encoded image features  $\mathbf{h}_i^r$ , thereby enhancing its ability to utilize rich reference information even when textual instructions are concise.

To handle multiple reference images, we introduce a positional offset for the reference-image tokens. Let the last token of the  $(i-1)$ -th reference image have position  $(n, m)$ . Then, the first token of the  $i$ -th reference image is assigned position  $(n+1, m+1)$ . This ensures that the position embeddings of reference-image tokens do not overlap across different references, which helps the DiT to distinguish multiple references during both training and inference.

### 3.3. Instruction-Reference Alignment

To achieve high-quality multi-subject generation, it is essential to resolve two prerequisite tasks in advance. First, the model must extract the subset of words in the editing instruction that correspond to the visual contents of the reference images. Second, for each such word, the model must localize the associated visual region within the corresponding reference image, typically represented as a bounding box.

To effectively address these challenges, we leverage the Vision-Language Model (VLM). For the first task, the reference images and the editing instruction are fed into the VLM, which outputs a set of referential words that correspond to visual subjects present in the reference images:

$$\mathcal{W} = [w_1, w_2, \dots, w_M] \quad (7)$$

where each  $w_j$  is a noun extracted from the instruction and confirmed to be visually grounded. For the second task, each referential word  $w_j$  is further processed by the VLM to determine its grounding in the reference set. Specifically, for each  $w_j$ , the VLM outputs the index of the corresponding reference image and its localized bounding box:

$$(\text{id}_j, [x_1^{(j)}, y_1^{(j)}, x_2^{(j)}, y_2^{(j)}]) \quad (8)$$

where  $\text{id}_j$  denotes the index of the reference image, and  $[x_1^{(j)}, y_1^{(j)}, x_2^{(j)}, y_2^{(j)}]$  denotes the bounding box (top-left and bottom-right coordinates).

During both training and inference, the VLM can extract these grounding cues solely based on the user-provided inputs. These outputs are then used to explicitly guide the attention computations in the DiT, alleviating the need for the DiT to implicitly solve the multimodal grounding task.

### 3.4. Correspondence-Aware Masked Attention

In the standard DiT attention layers, each text token from the VLM attends to all other tokens, which implicitly requires the DiT to perform *word-reference region correspondence reasoning*. This is challenging and suboptimal for a DiT pretrained on generic image generation tasks, as it is not explicitly trained for such multimodal grounding.

To address this, we leverage the pre-extracted word-bounding box pairs  $\{(w_j, \text{bbox}_j)\}_{j=1}^M$  to *directly guide the DiT attention computation*. Specifically, we locate all referential words  $w_j$  in the instruction and apply a masked attention that restricts their queries to relevant keys.

Let  $\mathbf{Q}_{\text{VLM}}^{w_j}$  denote the query corresponding to word  $w_j$ ,  $\mathbf{K}_{r, \text{bbox}_j}^{\text{VAE}}$  denote the keys of the reference-image VAE tokens inside bounding box  $\text{bbox}_j$ , and  $\mathbf{K}_{\text{VLM}}^e, \mathbf{K}_{\text{VAE}}^t$  denote the keys of the text VLM tokens and the target-image VAE tokens, respectively. The attention for word  $w_j$  is then computed as:

$$\mathbf{A}_{w_j} = \text{Softmax} \left( \frac{\mathbf{Q}_{\text{VLM}}^{w_j} [\mathbf{K}_{\text{VLM}}^e, \mathbf{K}_{\text{VAE}}^t, \mathbf{K}_{r, \text{bbox}_j}^{\text{VAE}}]^\top}{\sqrt{d}} \right) \times [\mathbf{V}_{\text{VLM}}^e, \mathbf{V}_{\text{VAE}}^t, \mathbf{V}_{\text{VAE}}^{r, \text{bbox}_j}], \quad (9)$$

where all irrelevant reference-image VAE tokens outside  $\text{bbox}_j$  and all reference-image VLM tokens are masked out.

This *Correspondence-Aware Masked Attention* mechanism allows the DiT to focus only on relevant multimodal associations, explicitly injecting the word-region correspondence into the attention process, while avoiding the need for DiT to implicitly solve the challenging grounding task. The correspondence between referential words and reference regions is explicitly encoded in the attention mechanism. As a result, when performing attention, the target-image VAE tokens can easily attend to the correct reference-image regions while following the guidance of the text tokens.

Formally, this establishes a binding between the textual instruction and the relevant reference regions, allowing the DiT to naturally extend its capability of following the text to also follow the reference image content. This mechanism enables the model to achieve both high text fidelity and high reference-image consistency in the generated results.

## 4. Experiments

### 4.1. Implementation Details

We build our method upon Qwen-Image-Edit (Wu et al., 2025a), a recent VLM+DiT framework designed for single-image editing. Since the original model only supports single-reference editing, we extend it to the multi-subject generation setting. During training, the VLM is frozen, while the DiT module is fully fine-tuned on a multi-subject dataset

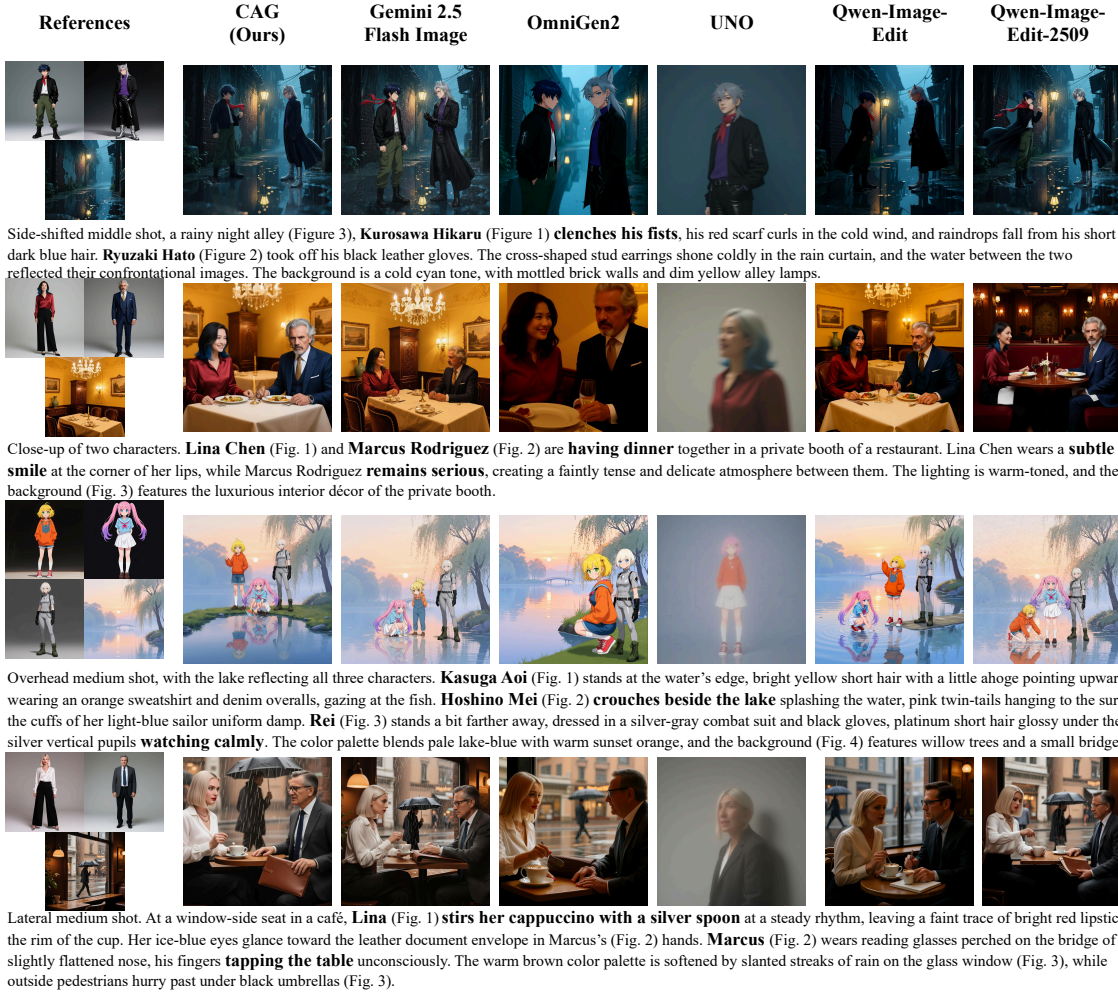


Figure 4. Qualitative comparison with different methods on multi-subject driven image generation.

containing approximately 24k examples with diverse character and scene references.

We employ the AdamW (Kingma & Ba, 2015) optimizer with a learning rate of 1e-5, training for 9k steps using a total batch size of 8. Following our design in Sec. 3, we apply a **VAE dropout** with a probability of 0.5. Additional ablation results on the VAE dropout probability are reported in the appendix. To support classifier-free guidance, we adopt a text dropout with a probability of 0.1. During inference, the number of denoising steps is set to 25, and the classifier-free guidance scale is set to 4.0. We utilize Qwen3-VL-30B-A3B-Instruct (QwenTeam, 2025) to extract *word-bounding box* pairs for both training and inference.

## 4.2. Evaluation Metrics

The test set contains 300 samples, each consisting of multiple reference subjects and one reference scene. Following OmniGen2 (Wu et al., 2025b) and VIEScore (Ku et al.,

2023), we employ the multi-modal model GPT-4.1 (OpenAI, 2025) to evaluate the quality of multi-subject image generation results. GPT-4.1 assesses each generated image along two dimensions: Prompt Following (PF) and Subject Consistency (SC), with scores ranging from 0 to 10. An Overall Score is further computed as the geometric mean of PF and SC, providing a balanced measure of both instruction adherence and subject fidelity. Following UNO (Wu et al., 2025c), we additionally report DINO, CLIP-I, and CLIP-T scores for completeness. DINO and CLIP-I measure subject similarity using cosine similarity between image-level features. However, these metrics provide limited explainability and are primarily designed for simple single-reference settings, making them inadequate for complex multi-subject generation. CLIP-T computes the cosine similarity between the prompt and the image CLIP embeddings, which is effective for short image captions but does not adequately capture the semantics of complex image editing instructions. Therefore, we mainly rely on **PF, SC, and Overall as the**

**primary evaluation metrics** for comparison, while DINO, CLIP-I, and CLIP-T are reported for reference.

### 4.3. Main Results

#### 4.3.1. QUANTITATIVE RESULTS

Table 1 reports the quantitative results on the multi-subject image generation task. Our method achieves the highest scores across all metrics, demonstrating superior ability in both instruction adherence and subject identity preservation. Specifically, our model attains 7.308 in Prompt Following (PF) and 7.906 in Subject Consistency (SC), leading to an Overall Score of 7.568. These results demonstrate that our approach establishes a new state of the art (SOTA) for multi-subject image generation.

When compared with OmniGen2 (Wu et al., 2025b) and Qwen-Image-Edit-2509 (Wu et al., 2025a), which share the VLM+DiT architectural design, our method achieves clear advantages. Specifically, our PF, SC, and Overall scores surpass OmniGen2 by +2.664, +1.862, and +2.326, respectively, and exceed Qwen-Image-Edit-2509 by +1.418, +1.293, and +1.390. Relative to our base model Qwen-Image-Edit (Wu et al., 2025a), our method improves PF by +1.709, SC by +1.187, and Overall Score by +1.494. This demonstrates the high quality of our generated results.

#### 4.3.2. QUALITATIVE RESULTS

Figure 4 presents the qualitative comparison results on the multi-subject image generation task. Our method demonstrates the best overall performance in both text alignment and reference consistency.

For instance, in the second row, Gemini 2.5 Flash Image, OmniGen2, and Qwen-Image-Edit exhibit noticeable discrepancies in the character’s hair color compared to the reference image. Qwen-Image-Edit-2509 produces inaccuracies in facial details and background consistency. By comparison, CAG better preserves fine-grained character-specific attributes while maintaining coherence with the reference background.

### 4.4. Ablation Studies

#### 4.4.1. EFFECTIVENESS OF PROPOSED METHODS

To verify the effectiveness of our proposed methods, we perform ablation experiments on the correspondence-aware masked attention and the VAE dropout training strategy, as shown in Table 2.

When only the correspondence-aware masked attention is applied, the model achieves a PF score of 7.063, an SC score of 7.853, and an Overall score of 7.415. Compared with the baseline (6.797 / 7.653 / 7.177), this corresponds to



A close-up side view: **Hino Haru** (Fig. 1) leans against a brick wall, strumming his guitar, the sleeves of his black leather jacket rolled up to reveal his forearms. **Hiro Debao** (Fig. 2) sits beside him on a wooden crate, unfolding a map, with a pencil clipped to the cuff of his orange shirt. The scene glows in warm yellow streetlight tones, and the background (Fig. 3) features an alley wall covered with old posters, while an empty beer can rolls beside the guitar case.

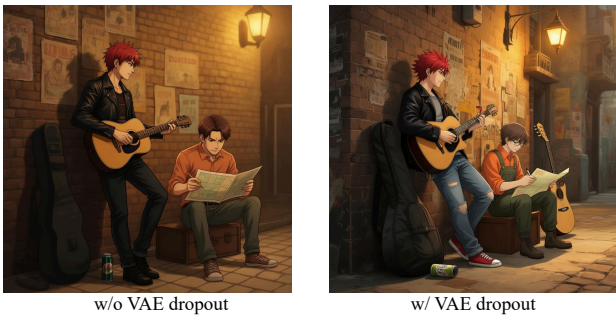


Figure 5. Qualitative comparison under inference **without using VAE features from reference images**. **w/o VAE dropout** denotes the model trained without the VAE dropout strategy and evaluated without reference-image VAE features, while **w/ VAE dropout** denotes the model trained with the VAE dropout strategy under the same inference setting.

improvements of +0.266, +0.200, and +0.238, respectively. By explicitly guiding each attention layer in DiT with the correspondence between textual tokens and reference image regions, the model effectively filters out irrelevant visual information, leading to better prompt adherence and subject consistency.

When only the VAE dropout strategy is used, the model achieves 7.177 in PF, 7.712 in SC, and 7.402 in Overall, outperforming the baseline by +0.380, +0.059, and +0.225, respectively. This shows that occasionally removing VAE features during training encourages DiT to depend more on VLM-derived semantic information, allowing it to capture details that are not explicitly mentioned in the text but are present in the reference images.

When both the correspondence-aware masked attention and the VAE dropout strategy are jointly applied, the model achieves the best overall performance with a PF score of 7.308, an SC score of 7.906, and an Overall score of 7.568. Their combination enables the model to achieve significant improvements in both prompt adherence and reference consistency.

As shown in Table 3, when VAE features are not used during inference, the model trained with the VAE dropout strategy achieves a PF score of 7.258 and an SC score of 7.354, resulting in an Overall score of 7.273. Compared to the model trained without VAE dropout (Overall 6.146), this represents a significant improvement of +1.127 in overall performance.

Method	PF↑	SC↑	Overall↑	DINO↑	CLIP-I↑	CLIP-T↑
Gemini 2.5 Flash Image (Google, 2025)	6.903	7.819	7.308	0.511	0.708	0.318
OmniGen2 (Wu et al., 2025b)	4.644	6.044	5.242	0.504	0.702	0.315
UNO (Wu et al., 2025c)	1.344	3.097	1.685	0.503	0.704	0.245
Qwen-Image-Edit (Wu et al., 2025a)	5.599	6.719	6.074	0.500	0.701	0.312
Qwen-Image-Edit-2509 (Wu et al., 2025a)	5.890	6.613	6.178	0.496	0.701	0.317
CAG (Ours)	<b>7.308</b>	<b>7.906</b>	<b>7.568</b>	<b>0.526</b>	<b>0.720</b>	<b>0.319</b>

Table 1. Comparison on the multi-subject image generation task. Each test sample contains multiple reference subjects and one reference scene. “PF” denotes Prompt Following. “SC” denotes Subject Consistency. Since Qwen-Image-Edit (Wu et al., 2025a) only supports single-image input, all reference images are concatenated into a single composite image to serve as input during inference.

Mask Attn.	VAE Dropout	PF↑	SC↑	Overall↑
✓		6.797	7.653	7.177
	✓	7.063	7.853	7.415
	✓	7.177	7.712	7.402
✓	✓	7.308	7.906	7.568

Table 2. Effectiveness of proposed methods. “Mask Attn.” denotes correspondence-aware masked attention. “VAE Dropout” denotes the VAE dropout training strategy. “PF” denotes Prompt Following. “SC” denotes Subject Consistency.

Method	PF↑	SC↑	Overall↑
w/o VAE dropout	6.591	5.807	6.146
w/ VAE dropout	7.258	7.354	7.273

Table 3. Quantitative comparison under inference **without using VAE features from reference images**. w/o VAE dropout denotes the model trained without the VAE dropout strategy and evaluated without reference-image VAE features, while w/ VAE dropout denotes the model trained with the VAE dropout strategy under the same inference setting.

As shown in Figure 5, when VAE features are not used during inference, the model trained without VAE dropout (left) produces incorrect details such as mismatched clothing and missing glasses. In contrast, the model trained with VAE dropout (right) generates results that accurately reproduce the reference clothing.

#### 4.4.2. VISUALIZATION OF TEXT-TO-REFERENCE ATTENTION MAPS

As shown in Figure 6, the attention maps between textual phrases and the VAE features of the reference images demonstrate that our proposed correspondence-aware masked attention enables the textual descriptions to accurately focus on their corresponding visual references.

In the example, when using Full Attn., the phrase “Hassan (Fig. 2)” exhibits dispersed attention over all reference images. Although part of the attention falls on the second reference image, the highlighted region is small and fails to

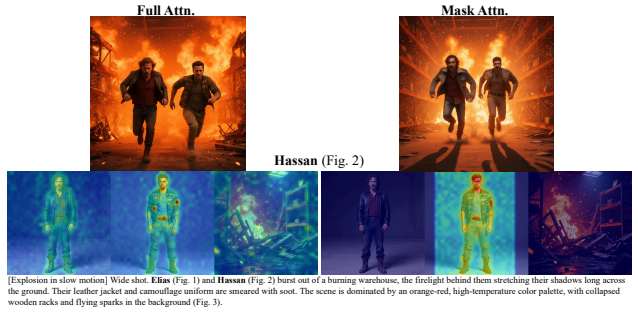


Figure 6. Visualization of attention maps from textual phrases to the VAE features of the reference images. “Full Attn.” denotes using full attention over all tokens, while “Mask Attn.” denotes our proposed correspondence-aware masked attention. The example visualizes the attention map for the phrase “Hassan (Fig. 2)”.

cover the entire face or the overall clothing of the character. In contrast, with Mask Attn., the attention of “Hassan (Fig. 2)” is sharply concentrated on the correct reference subject, particularly on the facial region, leading to noticeably improved subject consistency in the generated results.

## 5. Conclusion

In this work, we present **CAG**, a framework that couples high-level VLM semantics with low-level appearance cues. CAG prevents the DiT from being overloaded with multimodal understanding and can be readily incorporated into unified multimodal understanding-generation models.

Extensive experiments show that CAG achieves state-of-the-art performance in prompt following and subject consistency. Our findings highlight the value of combining conceptual and appearance-level guidance: high-level semantics provide stable, interpretable grounding, while low-level appearance cues preserve fine-grained subject details. This hierarchical synergy offers a promising direction for controllable and semantically grounded image generation in future unified architectures.

## References

Bai, S., Chen, K., Liu, X., Wang, J., Ge, W., Song, S., Dang, K., Wang, P., Wang, S., Tang, J., et al. Qwen2. 5-vl technical report, 2025.

Batifol, S., Blattmann, A., Boesel, F., Consul, S., Diagne, C., Dockhorn, T., English, J., English, Z., Esser, P., Kulal, S., et al. Flux. 1 kontext: Flow matching for in-context image generation and editing in latent space, 2025.

Bay, H., Tuytelaars, T., and Van Gool, L. Surf: Speeded up robust features. In *ECCV*, pp. 404–417, 2006.

Brooks, T., Holynski, A., and Efros, A. A. Instructpix2pix: Learning to follow image editing instructions. In *2023 IEEE/CVF Conference on Computer Vision and Pattern Recognition (CVPR)*, pp. 18392–18402, 2023. doi: 10.1109/CVPR52729.2023.01764.

Cao, S., Chen, H., Chen, P., Cheng, Y., Cui, Y., Deng, X., Dong, Y., Gong, K., Gu, T., Gu, X., et al. Hunyuuanimage 3.0 technical report, 2025.

Chen, B., Zhao, M., Sun, H., Chen, L., Wang, X., Du, K., and Wu, X. Xverse: Consistent multi-subject control of identity and semantic attributes via dit modulation. *arXiv preprint arXiv:2506.21416*, 2025a.

Chen, J., Xu, Z., Pan, X., Hu, Y., Qin, C., Goldstein, T., Huang, L., Zhou, T., Xie, S., Savarese, S., Xue, L., Xiong, C., and Xu, R. Blip3-o: A family of fully open unified multimodal models-architecture, training and dataset, 2025b. URL <https://arxiv.org/abs/2505.09568>.

Chen, X., Wu, Z., Liu, X., Pan, Z., Liu, W., Xie, Z., Yu, X., and Ruan, C. Janus-pro: Unified multimodal understanding and generation with data and model scaling, 2025c. URL <https://arxiv.org/abs/2501.17811>.

Cheng, Y., Wu, W., Wu, S., Huang, M., Ding, F., and He, Q. Umo: Scaling multi-identity consistency for image customization via matching reward, 2025. URL <https://arxiv.org/abs/2509.06818>.

Deng, C., Zhu, D., Li, K., Gou, C., Li, F., Wang, Z., Zhong, S., Yu, W., Nie, X., Song, Z., Shi, G., and Fan, H. Emerging properties in unified multimodal pretraining, 2025. URL <https://arxiv.org/abs/2505.14683>.

Gal, R., Alaluf, Y., Atzmon, Y., Patashnik, O., Bermano, A. H., Chechik, G., and Cohen-Or, D. An image is worth one word: Personalizing text-to-image generation using textual inversion. *arXiv preprint arXiv:2208.01618*, 2022.

Ge, Y., Zhao, S., Li, C., Ge, Y., and Shan, Y. Seed-data-edit technical report: A hybrid dataset for instructional image editing, 2024. URL <https://arxiv.org/abs/2405.04007>.

Google. Gemini 2.5 flash image. <https://developers.googleblog.com/en/introducing-gemini-2-5-flash-image/>, 2025.

Kingma, D. P. and Ba, J. Adam: A method for stochastic optimization. In *ICLR*, 2015.

Ku, M., Jiang, D., Wei, C., Yue, X., and Chen, W. Viescore: Towards explainable metrics for conditional image synthesis evaluation, 2023.

Lee, J., Kim, D., Ponce, J., and Ham, B. Sfnet: Learning object-aware semantic correspondence, 2019. URL <https://arxiv.org/abs/1904.01810>.

Lee, J., Kim, E., Lee, Y., Kim, D., Chang, J., and Choo, J. Reference-based sketch image colorization using augmented-self reference and dense semantic correspondence, 2020. URL <https://arxiv.org/abs/2005.05207>.

Li, H., Peng, X., Wang, Y., Peng, Z., Chen, X., Weng, R., Wang, J., Cai, X., Dai, W., and Xiong, H. Onecat: Decoder-only auto-regressive model for unified understanding and generation, 2025. URL <https://arxiv.org/abs/2509.03498>.

Lowe, D. G. Distinctive image features from scale-invariant keypoints. *IJCV*, 60:91–110, 2004.

Lu, J., Li, X., and Han, K. Regiondrag: Fast region-based image editing with diffusion models, 2024. URL <https://arxiv.org/abs/2407.18247>.

Mou, C., Wu, Y., Wu, W., Guo, Z., Zhang, P., Cheng, Y., Luo, Y., Ding, F., Zhang, S., Li, X., et al. Dreamo: A unified framework for image customization. *arXiv preprint arXiv:2504.16915*, 2025.

OpenAI. Gpt-4-1. <https://openai.com/index/gpt-4-1>, 2025.

Peebles, W. and Xie, S. Scalable diffusion models with transformers. In *Proceedings of the IEEE/CVF international conference on computer vision*, pp. 4195–4205, 2023.

QwenTeam. Qwen3-vl. <https://qwen.ai/blog?id=99f0335c4ad9ff6153e517418d48535ab6d8afe&from=research.latest-advancements-list>, 2025.

Ruiz, N., Li, Y., Jampani, V., Pritch, Y., Rubinstein, M., and Aberman, K. Dreambooth: Fine tuning text-to-image diffusion models for subject-driven generation. In *Proceedings of the IEEE/CVF conference on computer vision and pattern recognition*, pp. 22500–22510, 2023.

She, D., Fu, S., Liu, M., Jin, Q., Wang, H., Liu, M., and Jiang, J. Mosaic: Multi-subject personalized generation via correspondence-aware alignment and disentanglement, 2025. URL <https://arxiv.org/abs/2509.01977>.

Sheynin, S., Polyak, A., Singer, U., Kirstain, Y., Zohar, A., Ashual, O., Parikh, D., and Taigman, Y. Emu edit: Precise image editing via recognition and generation tasks, 2023. URL <https://arxiv.org/abs/2311.10089>.

Tan, Z., Liu, S., Yang, X., Xue, Q., and Wang, X. Ominicontrol: Minimal and universal control for diffusion transformer. In *ICCV*, 2025.

Tang, L., Jia, M., Wang, Q., Phoo, C. P., and Hariharan, B. Emergent correspondence from image diffusion, 2023. URL <https://arxiv.org/abs/2306.03881>.

Team, C. Chameleon: Mixed-modal early-fusion foundation models, 2025. URL <https://arxiv.org/abs/2405.09818>.

Wang, P., Bai, S., Tan, S., Wang, S., Fan, Z., Bai, J., Chen, K., Liu, X., Wang, J., Ge, W., et al. Qwen2-vl: Enhancing vision-language model's perception of the world at any resolution, 2024.

Wu, C., Li, J., Zhou, J., Lin, J., Gao, K., Yan, K., Yin, S.-m., Bai, S., Xu, X., Chen, Y., et al. Qwen-image technical report, 2025a.

Wu, C., Zheng, P., Yan, R., Xiao, S., Luo, X., Wang, Y., Li, W., Jiang, X., Liu, Y., Zhou, J., et al. Omnipgen2: Exploration to advanced multimodal generation. *arXiv preprint arXiv:2506.18871*, 2025b.

Wu, S., Huang, M., Wu, W., Cheng, Y., Ding, F., and He, Q. Less-to-more generalization: Unlocking more controllability by in-context generation, 2025c. URL <https://arxiv.org/abs/2504.02160>.

Xia, B., Wang, S., Tao, Y., Wang, Y., and Jia, J. Llmga: Multimodal large language model based generation assistant, 2024. URL <https://arxiv.org/abs/2311.16500>.

Xia, B., Peng, B., Zhang, Y., Huang, J., Liu, J., Li, J., Tan, H., Wu, S., Wang, C., Wang, Y., et al. Dreamomni2: Multimodal instruction-based editing and generation, 2025.

Zhang, J., Herrmann, C., Hur, J., Cabrera, L. P., Jampani, V., Sun, D., and Yang, M.-H. A tale of two features: Stable diffusion complements dino for zero-shot semantic correspondence, 2023a. URL <https://arxiv.org/abs/2305.15347>.

Zhang, J., Herrmann, C., Hur, J., Chen, E., Jampani, V., Sun, D., and Yang, M.-H. Telling left from right: Identifying geometry-aware semantic correspondence, 2024. URL <https://arxiv.org/abs/2311.17034>.

Zhang, K., Mo, L., Chen, W., Sun, H., and Su, Y. Magicbrush: a manually annotated dataset for instruction-guided image editing. In *Proceedings of the 37th International Conference on Neural Information Processing Systems*, NIPS '23, Red Hook, NY, USA, 2023b. Curran Associates Inc.

## Appendix

### A. Details of Instruction-Reference Alignment

Instruction-reference alignment comprises two subtasks: (i) identifying words that are semantically grounded in the reference images, and (ii) localizing the corresponding visual regions for each identified word. Figure 7 illustrates the prompt used to extract reference-related words from the editing instruction, while Figure 8 presents the prompt used to predict the bounding boxes associated with each extracted word. We use Qwen3-VL-30B-A3B-Instruct (QwenTeam, 2025) for the Instruction-Reference Alignment. As shown in Figure 9, the VLM first parses the editing instruction and extracts all nouns that correspond to the reference images. It then localizes the visual regions associated with each extracted word. The images at the bottom visualize these grounded regions on the reference images.

### B. Ablation on VAE Dropout Probability

With Correspondence-Aware Masked Attention enabled, we train our model using varying VAE dropout probabilities. As shown in Figure 10, the PF, SC, and Overall scores (Wu et al., 2025b) exhibit a consistent trend: moderate dropout yields the best performance across all metrics. Performance improves as the dropout probability increases from 0 to the mid range, reaching its peak around 0.3–0.5. Beyond this point, all three metrics decline noticeably as the dropout probability continues to rise. Specifically, the PF and Overall scores peak at a dropout probability of 0.5, while the SC score peaks at a dropout probability of 0.3. Training with randomly dropped VAE features encourages the model to rely more heavily on the fine-grained semantic cues encoded in the VLM features, though excessive dropout weakens its ability to utilize detailed VAE-based appearance information. An appropriate dropout probability therefore enables the model to effectively balance these two feature sources, leading to consistent improvements in both prompt following and subject consistency.

### C. More Results

We present additional visualizations produced by CAG in Figure 11, Figure 12, and Figure 13. The results show that CAG faithfully follows the action descriptions specified in the editing instructions and places multiple characters coherently within the scene defined by the reference images. Moreover, CAG adapts the global composition according to the viewpoint directives in the instruction, demonstrating strong controllability over scene layout. The generated images also exhibit high subject consistency, preserving all fine-grained appearance details of each referenced character. These observations collectively validate the effective-

ness of our VAE dropout training strategy and the proposed Correspondence-Aware Masked Attention.

<Image>ref\_image1</Image><Image>ref\_image2</Image><Image>ref\_image3</Image>

Your task is to identify and extract all character and clothing names that appear in the reference images from the description. Make sure not to include any adjectives or nouns that are unrelated to characters, such as "background."

Please follow these instructions:

List all character and clothing names in the order they appear in the description. Preserve the exact wording of each character or clothing name exactly as it appears in the description.

**Example 1:**

"Oblique side view from above, close-up. Rin (Fig.1) has ice-blue short hair falling over her shoulders, her brows slightly furrowed, and her left hand offering a light-blue ice cream that is about to melt; the ice-crystal-gloss strands of her hair are dotted with tiny droplets. Xi (Fig.2) has bouncing pink twin-tails, her round face with eyes curved like crescents, holding the ice cream with both hands; the hem of her pink Lolita dress is stained with grass. The background is a bright yellow ice-cream truck (Fig.3), with interwoven pink-blue tones and white halftone-paper effects along the edges of the frame."

Your output should be a list of names, as follows:

['Rin (Fig.1)', 'ice-blue short hair', 'ice-crystal-gloss strands', 'Xi (Fig.2)', 'pink twin-tails', 'round face', 'pink Lolita dress']

**Example 2:**

"Oblique long shot. Cang (Fig.1) is running across a golden beach while carrying Xi (Fig.2) on their back; the sea-blue gradient short hair is tinted orange-red by the sunset, the hem of the blue-white striped shirt flutters in the wind, and the right hand grabs Xi (Fig.2)'s pink Lolita dress hem. Xi (Fig.2) lies on Cang (Fig.1)'s back, her pink twin-tails hanging down on both sides of Cang (Fig.1)'s shoulders, her round face with eyes tightly shut, drooling at the mouth, holding a glowing star prop in her hand. The background is the ocean surface under an orange-yellow sunset (Fig.3), with a string of uneven footprints left on the beach (Fig.3), and crescent-shaped waves (Fig.3) hitting the shore."

Your output should be a list of names, as follows:

['Cang (Fig.1)', 'Xi (Fig.2)', 'sea-blue gradient short hair', 'blue-white striped shirt', 'pink Lolita dress hem', 'pink twin-tails']

Now, given the following description, extract the list of names in the same format:

<Instruction>

*Figure 7.* Prompt used to extract words associated with the reference images.

```
<Image>ref_image1</Image><Image>ref_image2</Image><Image>ref_image3</Image>
```

Draw a bounding box around the location of each object in the list, and output in JSON format which image each object is in and its bbox coordinates.

The JSON format is as follows:

```
[  
  {"image_id": "1,2,3,...", "bbox_2d": [x1, y1, x2, y2], "label": "object name"},  
  {"image_id": "1,2,3,...", "bbox_2d": [x1, y1, x2, y2], "label": "object name"},  
  ...  
]
```

The list is as follows:

```
<object_list>
```

*Figure 8.* Prompt used to obtain the bounding boxes corresponding to each word.

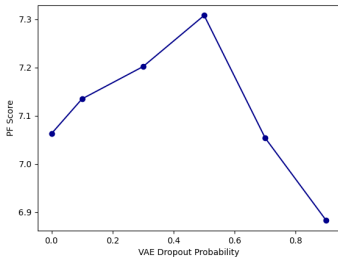
Tracking shot at the schoolyard basketball hoop. Kazama Che (Fig.1) dribbles the ball and breaks through Akai Kenji (Fig.2)'s defense, the sleeves of his black leather jacket rolled up to his elbows, his light-blue short hair whipping as he makes a sudden stop. Akai Kenji (Fig.2)'s yellow sleeveless top stretches over his muscles, and his army-green work pants slip down to his knees; as he reaches out to steal the ball, a corner of the bandage on his arm comes loose. The color tone is the orange-red sunset, and the background is the chain-link fence and the basketball hoop (Fig.3) casting long shadows.

["Kazama Che (Fig.1)", "Akai Kenji (Fig.2)", "black leather jacket", "light-blue short hair", "yellow sleeveless top", "army-green work pants", "bandage"]

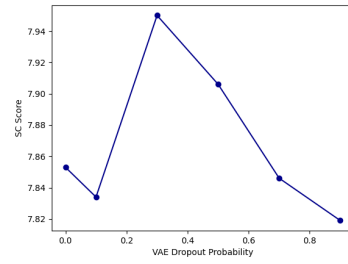
```
[{"image_id": "1", "bbox_2d": [300, 14, 655, 987], "label": "Kazama Che (Fig.1)"}, {"image_id": "2", "bbox_2d": [311, 24, 643, 973], "label": "Akai Kenji (Fig.2)"}, {"image_id": "1", "bbox_2d": [323, 163, 655, 555], "label": "black leather jacket"}, {"image_id": "1", "bbox_2d": [405, 14, 563, 130], "label": "light-blue short hair"}, {"image_id": "2", "bbox_2d": [419, 185, 576, 398], "label": "yellow sleeveless top"}, {"image_id": "2", "bbox_2d": [360, 401, 641, 815], "label": "army-green work pants"}, {"image_id": "2", "bbox_2d": [571, 397, 633, 545], "label": "bandage"}]
```



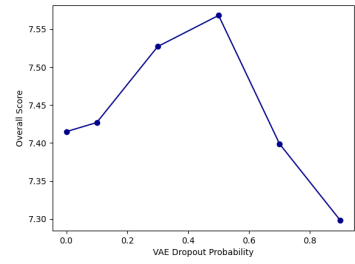
Figure 9. Example of Instruction-Reference Alignment.



(a) PF scores.



(b) SC scores.



(c) Overall scores.

Figure 10. Curves of PF, SC, and Overall scores under varying VAE dropout probabilities.



A front-facing medium shot at a window-side café table: Rin Kiryu (Fig. 1) has her wine-red long hair draped over a white knitted cardigan as she lifts a piece of strawberry cake toward Yuna Mizuno (Fig. 2). Yuna's green eyes brighten as she cups a ceramic coffee mug in both hands. Soft, creamy warm-white lighting falls across the wood-grain table, while the background (Fig. 3) shows street trees outside the glass window.



A top-down medium shot: Marcus (Fig. 1) and Lina (Fig. 2) sit together on a leather sofa in the corner of a café. Marcus's khaki jacket is draped over the back of the seat, and his gray graphic T-shirt shows a faded band logo. Lina wears light-blue denim overalls, the cuffs rolled up to reveal a silver star anklet catching the light. The atmosphere is warm brown and relaxed, with the background (Fig. 3) featuring a frosted wooden round table and steaming ceramic cups.



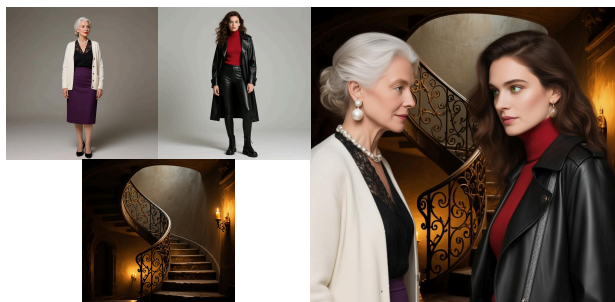
Oblique close-up: Chen Jing (Fig. 1) and Wang Qiang (Fig. 2) stand at the café bar counter. Chen Jing's beige heeled sandals lift her slightly onto her toes, her white shirt collar slightly open, and the latte in her hand letting off steam. Wang Qiang's black work jacket has its sleeves rolled up, and his silver ring taps against his black-coffee cup. The two lean in and speak quietly. The color palette is mature and restrained, dominated by beige, black, and brown. The background shows the café's wooden bar counter and the burlap coffee-bean sacks hanging on the wall (Fig. 3).



Medium eye-level shot: In front of a street graffiti wall (Fig. 4), A-Zheng (Fig. 1) bends forward while painting, holding a spray can; his black leather jacket hangs open to reveal a silver necklace, and the ripped jeans have exaggerated frayed lines at the knees. Lili (Fig. 2) hands him a purple paint can, her magenta ponytail brushing across her cheek, and the plaid shirt tied around her waist flutters with her movement. A-Shu (Fig. 3) crouches on the ground sketching the base lines with a pencil, hoodie sleeves rolled up to his elbows. The background graffiti is composed of bold lines and color blocks, with striking red-purple-blue contrasts.



Side-view medium shot: Lin Wanying (Fig. 1) holds out a snow-dusted cherry-blossom branch toward Kazama Che (Fig. 2). Her pink puff-sleeve dress is dusted with petals, while he gazes down at the branch, his light-blue eyes lowered. The color palette is pink and white, and the background features a bench covered in fallen cherry blossoms (Fig. 3). Fine lines depict her fluttering twin ponytails and his tousled short hair.



Close-up: The swaying pearl earring of Sophia (Fig. 1) moves in the same frame as the metallic zipper on Evelyn's (Fig. 2) trench coat collar. Sophia's light-blue eyes gaze gently into Evelyn's green eyes. The background features the wrought-iron railing of a spiral staircase (Fig. 3), with candlelight spilling from a wall sconce. The overall tone is dark gold, reminiscent of a medieval oil painting.

Figure 11. Generated samples from CAG.



Eye-level medium shot. At a round table in a café, Lin Xiaoyu (Fig. 1) hands a cup of coffee to Chen Xue (Fig. 2), the sleeve of her pink T-shirt stained with a bit of milk foam. Chen Xue (Fig. 2) takes the cup, a small badge pinned to the collar of her white shirt, and the two share a warm smile. In a cozy warm-brown palette, the background (Fig. 3) features wooden tables and chairs and small decorative paintings on the wall, with rounded lines emphasizing the curve of the cup and fine strokes outlining the characters' facial expressions.



A side-view medium shot: Enji (Fig. 1) leans against the wall of an abandoned train station, his leather jacket slipping down his arms, an unlit cigarette held between the fingers of his right hand. His amber beast-like eyes lift in a raised-brow glance toward Kagekage (Fig. 2). Kagekage stands opposite him, trench coat unbuttoned, left hand in his pocket, his dark-red left eye sharp as if engaged in a tense conversation. The background (Fig. 3) shows rusted rails stretching into the distance, a signal light blinking red, the scene cast in dark blue and black tones, with a faint glow shimmering far away.



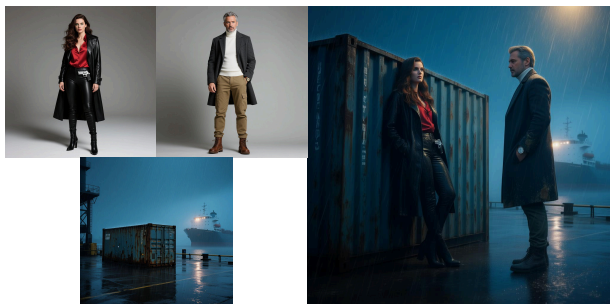
An over-the-shoulder medium shot: Marcus Rodriguez (Fig. 1) and Zoe Harper (Fig. 2) sit in the corner of a café. Marcus slides an envelope across the table toward her, and Zoe picks it up, her fingers trembling slightly. Soft natural light fills the scene, while the background (Fig. 3) shows autumn leaves drifting down outside the window.



Pull-back medium shot. Deep inside an underground passage, Sato Kenji (Fig. 1) and Yamamoto Ryu (Fig. 2) stand back-to-back — Kenji's red jacket zipped all the way up, while Ryu's black leather jacket hangs open, revealing a white tank top. Both turn their heads simultaneously toward opposite ends of the corridor, the green highlights in Kenji's hair contrasting sharply with Ryu's golden ponytail under the cold blue-gray glow of the emergency lights. The background (Fig. 3) shows walls covered with faded street graffiti.



A low-angle medium shot: Beside the faded wooden door of an old bookstore, Kane (Fig. 1) rests the dusty cuff of his khaki trench coat against the doorframe. Sophia (Fig. 2) wears a dark red knitted cardigan, its neckline revealing an amber pendant. Both of them gaze toward the shop window, where piles of old books rise like a small mountain. The scene (Fig. 3) carries a vintage brown-yellow tone, with a rusted sign reading "Established 1983" and a brick wall overgrown with ivy in the background.



On a rainy night at the docks (Fig. 3), a low-angle medium shot: Evelyn (Fig. 1) leans against a rusted shipping container, her black leather trench coat soaked by the rain, the outline of her holstered handgun clear at her waist. Kane (Fig. 2) stands opposite her, the hem of his dark gray wool coat speckled with mud, while the dial of his old mechanical watch flashes with a cold glint under the dim streetlamp. The palette is in cold blue tones, with the background showing the fog lights of a distant cargo ship diffusing through the rain, as slanting raindrops sweep past the lens.

Figure 12. Generated samples from CAG.



Top-down close-up: In front of the wooden easel in the studio, Ayue (Fig. 1) leans over to look at Weizai's (Fig. 2) sketchbook, her light-brown shoulder-length hair falling to the edge of the paper, the neckline of her white T-shirt slightly open. Weizai's (Fig. 2) hand holding the pencil pauses on the page, gray-blue short hair covering his narrow eyes, and the cuff of his black leather jacket is stained with paint. On the sketchbook is a city silhouette outlined with fine lines. In the background, unfinished watercolor drafts are pinned to the easel. The overall tone is cool gray with hints of ochre, matching the scene (Fig. 3).



Low-angle, upward full shot. At the edge of the basketball court, Ache (Fig. 1) jumps high, preparing to shoot, the back of his white hoodie stained with bits of grass, his ink-blue short hair damp with sweat. Xiaotang (Fig. 2) crouches at the sidelines holding up a bottle of mineral water, the hem of her yellow pinafore dress smudged with dust. Awei (Fig. 3) stands with hands on hips nearby, his leather jacket open to reveal gray cargo pants as he grins and shouts encouragement. The scene is bright white in tone, with harsh afternoon sunlight reflecting off the ground. The background features a chain-link fence and the silhouette of a distant school building (Fig. 4).



Side-angle medium shot at the school gate (Fig. 3), dominated by warm yellow tones, with cherry blossoms drifting down. Tsukishima Umi (Fig. 2) stands on tiptoe to hand a star-shaped hair accessory to Tachibana Yukino (Fig. 1); the sway of Umi's pink dress catches light on her pearl necklace, while Yukino's sailor-uniform collar and school emblem gently move with her motion. The background features the stone school gate engraved with the school motto.



Side-follow medium shot: In the rain-soaked alley at night, neon lights shimmer in the puddles. Ranche (Fig. 1) holds a long black umbrella, his crow-green short hair dotted with water droplets, amber eyes fixed intently ahead. Liuli (Fig. 2) walks on the right side, her deep-purple haori blown open by the wind, indigo long hair clinging to her neck. A pale-cyan totem at the bridge of her nose glows faintly under the streetlamp. Her wooden clogs step through a puddle, sending ripples outward. The background features old shops on both sides hung with rows of red lanterns (Fig. 3).



Front-facing medium shot. Ice-spike Kaine (Fig. 1) stands with the hem of his blue robe frozen over, while Fire-caster Lina (Fig. 2) unleashes flames from both hands. Ice-blue and warm orange tones clash dramatically, with bold strokes outlining the flowing motion of Kaine's silver-white icy hair and Lina's fiery red hair. The background is a fractured ground where ice and fire intertwine (Fig. 3).



Wide shot, high-angle top view. On a construction site under a torrential downpour, Marcus (Fig. 1) wears a safety helmet, his olive-green work jacket darkened by the rain, his commanding hand gestures sharp and forceful. Cain (Fig. 2) walks through the mud, the hem of his dark gray coat sweeping the ground; a black umbrella hides half his face, and the collar of his white shirt is stained darker by the rain. In a cold blue-gray palette, the background (Fig. 3) features towering cranes and the skeletal concrete frame of an unfinished building.

Figure 13. Generated samples from CAG.